

## Plasma Electrolytic Oxidation of Tantalum\*

Marija Petković<sup>1</sup>, Stevan Stojadinović<sup>1</sup>, Rastko Vasilic<sup>2</sup>,  
Ivan Belča<sup>1</sup>, Bećko Kasalica<sup>1</sup>, Ljubiša Zeković<sup>1</sup>

**Abstract:** This paper is a review of our research on the plasma electrolytic oxidation (PEO) process of tantalum in 12-tungstosilicic acid. For the characterization of microdischarges during PEO, real-time imaging and optical emission spectroscopy (OES) were used. The surface morphology, chemical and phase composition of oxide coatings were investigated by AFM, SEM-EDS and XRD. Oxide coating morphology is strongly dependent on PEO time. The elemental components of PEO coatings are Ta, O, Si and W. The oxide coatings are partly crystallized and mainly composed of  $WO_3$ ,  $Ta_2O_5$  and  $SiO_2$ .

**Keywords:** Tantalum, Plasma electrolytic oxidation (PEO); 12-tungstosilicic acid.

### 1 Introduction

Plasma electrolytic oxidation (PEO) is an economic, efficient and environmentally benign technology capable of producing *in-situ* oxide coatings on aluminum, magnesium, titanium, zirconium, tantalum, and other light metals as well as on their alloys. Oxide coatings have controllable morphology and composition, excellent bonding strength with the substrate, good electrical and thermal properties, high microhardness and high-quality wear and corrosion resistance [1 – 3]. Consequently, PEO oxide coatings are highly desirable for applications in textile industry, aerospace, automotive engineering, biomedical devices, etc. [4 – 7].

PEO is a complex process combining concurrent partial processes of oxide layer formation, dissolution and dielectric breakdown. At the beginning of the anodic process thin barrier oxide layer is formed on the substrate [8]. Barrier oxide layer is produced at both the metal/oxide and oxide/electrolyte interfaces as a result of migration of  $O^{2-}/OH^-$  and ions of metal across the oxide assisted by a high electric field. Also, small amounts of anionic components of electrolyte are incorporated into the oxide at the oxide/electrolyte interface during the anodization. Barrier oxide layers are amorphous and have ionic conductivity

---

<sup>1</sup>Faculty of Physics, University of Belgrade, Studentski trg 12, 1000 Belgrade, Serbia;  
E-mail: marijapetkovic@ff.bg.ac.rs.

<sup>2</sup>Faculty of Environmental Governance and Corporate Responsibility, Educons University, Sremska Kamenica

\*Award for the best paper presented in Section *New Materials*, at Conference ETRAN 2011, June 6-9, Banja Vrućica – Teslić, Bosnia and Herzegovina.

and high electrical resistance. Thickness of barrier oxide layer is limited to several hundred nanometers due to the dielectric breakdown under high electric field, followed by intense generation of spark discharges over the coating surface, accompanied by gas evolution. The anodic gas consists predominantly of oxygen with minor fractions of other elements. A number of separated discharge channels occur at flaws in the oxide coating [9], and high local current densities are generated at the flaw site prior to healing of the defect and termination of the microdischarges. The microdischarging results in localized high temperature and high pressure, allowing for formation of oxide coatings consisting of not only predominant substrate oxides but of more complex oxides containing compounds which involve the components present in the electrolyte [10].

In this paper, we have investigated PEO process of tantalum in 12-tungstosilicic acid. Tungsten-containing oxide layers on tantalum are of interest because of their catalytic, semiconducting and corrosion-resistant properties. The microdischarge characteristics during PEO process of tantalum were investigated by optical emission spectroscopy and real-time imaging. Physicochemical methods: atomic force microscopy (AFM), scanning electron microscopy (SEM-EDS) and x-ray diffraction (XRD) served as tools for examining surface morphology, chemical and phase composition of obtained oxide coatings.

## **2 Experimental**

In the experiment, oxide coatings were formed on tantalum samples of dimensions  $(25 \times 5 \times 0.125) \text{ mm}^2$  and 99.9 % purity. Before the anodization, tantalum was degreased in acetone, ethanol and distilled water, using ultrasonic cleaner, and dried in a warm air stream. The oxidation process was carried out in an electrolytic cell. Two platinum wires (5 cm long and 1 mm in diameter) were used as cathodes. For anodization of tantalum we used water solution of 0.001 M (pH = 2.8) 12-tungstosilicic acid ( $\text{H}_4\text{SiW}_{12}\text{O}_{40}$ ). The electrolyte was prepared using double distilled and deionized water and PA (pro analysis) grade chemical compound. Anodizing was carried out at current density of  $70 \text{ mA/cm}^2$ . During the anodization, the electrolyte circulated through the chamber-reservoir system. The temperature of the electrolyte was maintained during the anodization process at  $(21 \pm 1) \text{ }^\circ\text{C}$ . After the anodization, samples were rinsed in distilled water to prevent additional deposition of electrolyte components during drying.

Spectral characterization of PEO was performed utilizing a spectrograph system based on the Intensified Charge Coupled Device (ICCD) camera intended for time-resolved measuring of very weak light intensity in a wide range of wavelengths [11]. Optical detection system consisted of a large-

aperture achromatic lens, a Hilger spectrograph with diffraction grating 1200 grooves/mm (wavelength range of 43 nm) and a very sensitive PI-MAX ICCD cooled camera with high quantum efficiency manufactured by Princeton Instruments. The system is used with several grating position with over-lapping wavelength range of 10 nm. The CCD chip consisted of 1024×256 pixels, each approximately 26×26  $\mu\text{m}$ . To reduce the dark current the CCD chip is cooled at  $-40\text{ }^\circ\text{C}$  using Peltier devices. The optical-detection system was calibrated using light emitting diodes (LEDs) based light source [11]. The obtained spectra were adjusted to the spectral response of the measuring system. Real-time images during PEO were recorded utilizing a video camera Sony DCR-DVD110 (800K pixels CCD, 40× optical zoom and 40 mm lens filter). The information obtained was split into separate frames and the images of individual frames were processed using our custom made software, which automatically counted microdischarges in selected frames, determined spatial density, and dimensional distribution of the microdischarges.

The morphology of surface coatings was characterized using an atomic force microscope (AFM; Veeco Instruments, model Dimension V). Micrographs were obtained in tapping mode under ambient conditions, using TAP300 tips (resonant frequency 300 kHz, force constant 40 N/m). Scanning electron microscope (SEM) JEOL 840A equipped with energy dispersive x-ray spectroscopy (EDS) was used to characterize chemical composition of formed surface coatings. The crystallinity of samples was analyzed by XRD, using a Phillips PW 1050 powder diffractometer in Bragg-Brentano geometry, with Ni-filtered  $\text{CuK}_\alpha$  radiation. Diffraction data were acquired over scattering angle  $2\theta$  from 10 to  $80^\circ$  with a step of  $0.050^\circ$  and acquisition time of 1 s/step.

### 3 Results and Discussion

#### 3.1 Optical characterization and morphology of PEO coatings

Voltage-time response during galvanostatic anodization of tantalum in 0.001 M 12-tungstosilicic acid at constant current density of  $70\text{ mA/cm}^2$  is shown in Fig. 1. From the beginning of anodization, the voltage increases approximately linearly with time to about 420 V in a very short time with average slope of 16.7 V/s resulting in the constant rate of increase of the oxide film thickness. This stage is followed by apparent deflection from linearity in voltage-time curve, starting from so-called sparking (breakdown) voltage. After the breakdown, voltage continually increases, but the voltage-time slope decreases and a large number of small size microdischarges appear, evenly distributed over the whole sample surface. Further anodization results in relatively stable value of the voltage of anodization.

Based on the voltage-time response, the PEO process can be divided in three stages. During the anodization of tantalum, total current density is the sum

of ionic current density and of electron current density. In the first stage, the electric field strength for a given current density remains constant during the anodic growth and the ionic current is two to three orders of magnitude larger than the electronic component. In order to maintain the constant electric field strength, the voltage of anodization must increase linearly as the film thickens. Also, during anodization electrons are injected into the conduction band of the anodic oxide and accelerated by the electric field producing avalanches by an impact ionization mechanism. When the avalanche electronic current reaches critical value the breakdown occurs. In the next stage a relatively low voltage is required to maintain the same total current density (compared with the first stage), due to the independence of electron current density with anodic oxide film thickness. In the last stage, the fraction of electron current density in total current density becomes the dominant one. In this stage, the total current density is almost independent of the anodic oxide film thickness and the voltage-time slope is close to zero.

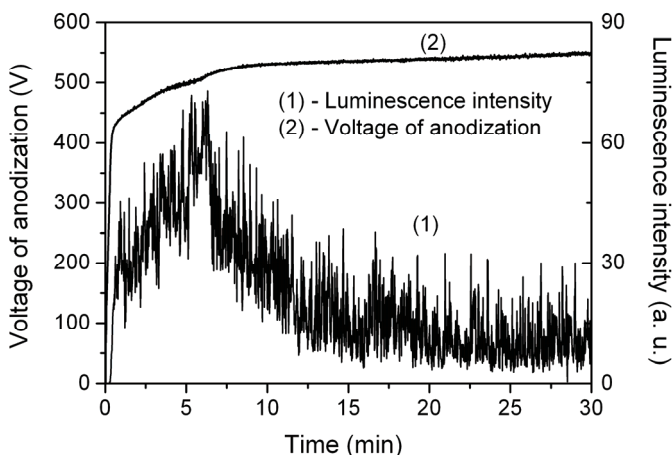


**Fig. 1** – Time variation of voltage and luminescence intensity at 450 nm during galvanostatic anodization of tantalum in 12-tungstosilicic acid.

AFM micrographs of the oxide surface before and after breakdown are shown in Fig. 2. Before breakdown the relatively compact barrier oxide films are formed (Fig. 2a). After breakdown the oxide surface becomes laced with a number microdischarge channels as well as molten regions formed due to rapid cooling effect of the electrolyte (Figs. 2b-d). Breakdown of the oxide films is triggered by local heating effects caused by highly localized processes taking place at macro and microdefects in the oxide (electrolyte-filled fissures, micropores, flaws, etc.). In a thicker layer of oxide coating, higher energy is required for the current to pass through the coating. Under this condition, the

current is localized at weak points of the layer formed to find its way through the coating. Consequently, the diameter of the discharge channel increases.

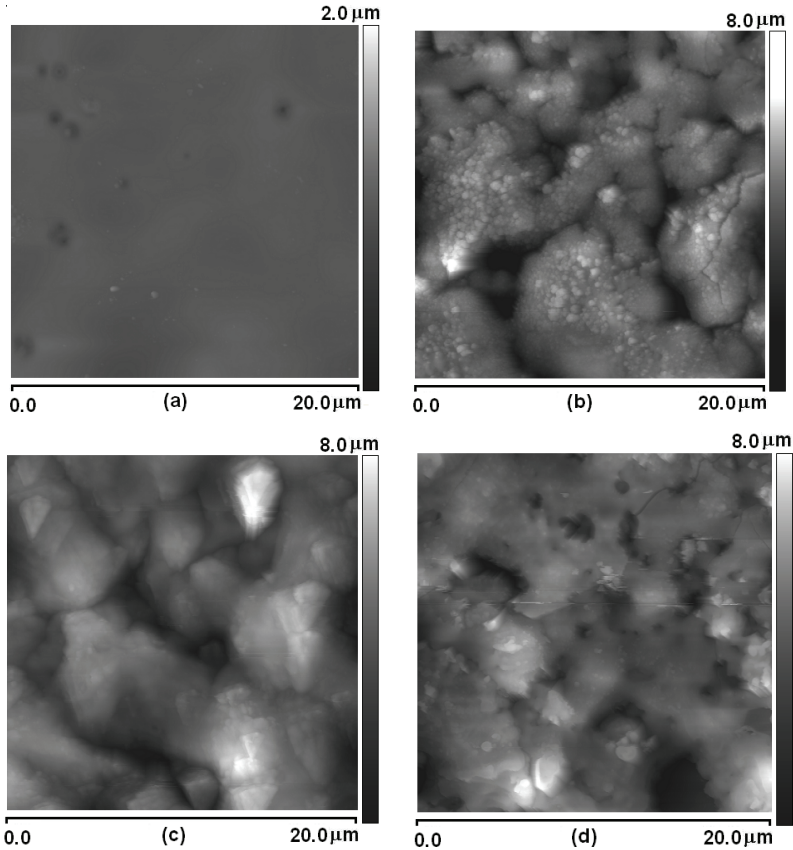


**Fig. 2** – AFM micrographs of oxide coatings formed in 12-tungstosilicic acid at various stages of PEO process: (a) 15 s; (b) 3 min; (c) 15 min; (d) 30 min.

Real time imaging revealed several stages of the PEO process (Fig. 3), with distinct microdischarge characteristics. Intensive gas generation is observed after first few seconds of anodization (Fig. 3a). Small microdischarges, with average cross-sectional area  $\sim 0.05 \text{ mm}^2$ , are visible after about 20 s, together with gas bubble evolution (Fig. 3b). During the PEO the size of microdischarges becomes larger, while the number of microdischarges is reduced.

The evolution of the microdischarge spatial density is shown in Fig. 4a. Spatial density of microdischarges is the largest after about 2.5 min from the beginning of PEO process, than it reduces substantially during next 5 min from about  $225 \text{ cm}^{-2}$  to  $50 \text{ cm}^{-2}$ , and than stays almost constant. The percentage of oxide coating area, simultaneously covered by active discharge sites has also

maximum after 2.5 min from the beginning of the PEO process (~5 %) and then monotonically decreases with the time of PEO processing (Fig. 4b).

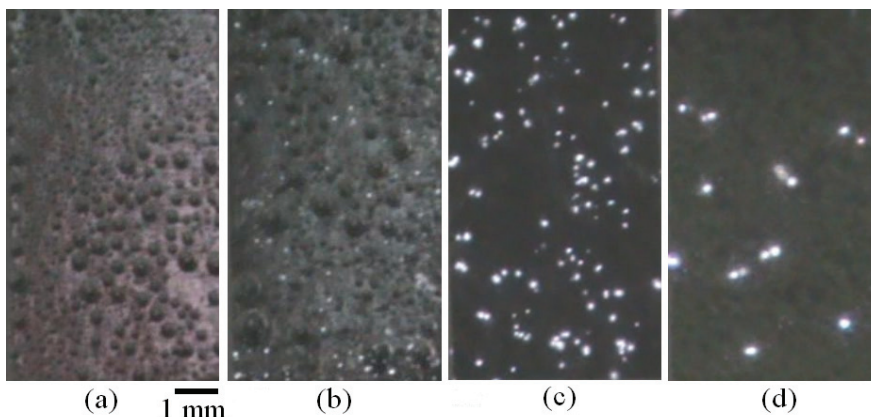


**Fig. 3** – *Microdischarges appearance at various stages of PEO process: (a) 10 s; (b) 20 s; (c) 3 min; (d) 30 min.*

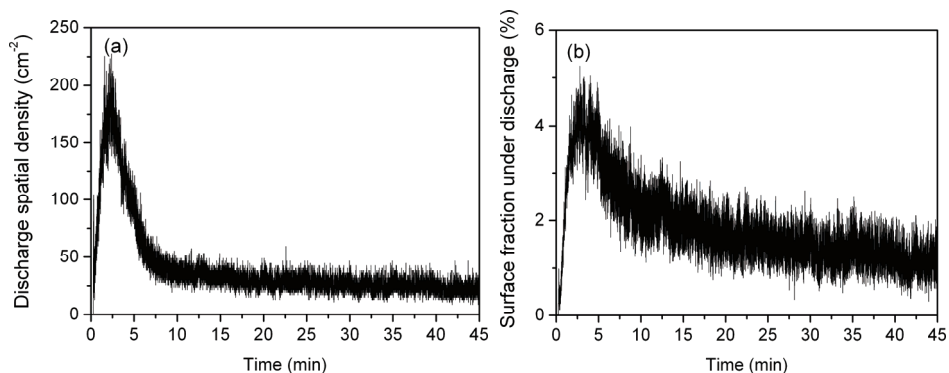


**Fig. 4** – *Microdischarge characteristics at various stages of PEO process: (a) Microdischarge spatial density; (b) Percentage of oxide coating area simultaneously covered by active discharge sites.*

The dimensional distribution of PEO microdischarges is shown in Fig. 5. Relatively small microdischarges (cross-sectional area  $< 0.1 \text{ mm}^2$ ) are present throughout the whole PEO process. Their concentration reaches almost 100 % of the total population at the beginning of PEO (Fig. 5a), and decreases to about 75 % during the final stages of the treatment (Fig. 5f). The portion of medium-size microdischarges (cross-sectional area from  $0.1 \text{ mm}^2$  to  $0.2 \text{ mm}^2$ ) is negligible at the beginning of the PEO process, but increases considerably with PEO time, reaching a maximum value of 32 % after about 10 min, and

decreases to 17 % in the final stage. Large microdischarges (cross-sectional area  $> 0.2 \text{ mm}^2$ ) become noticeable only after extended PEO times.

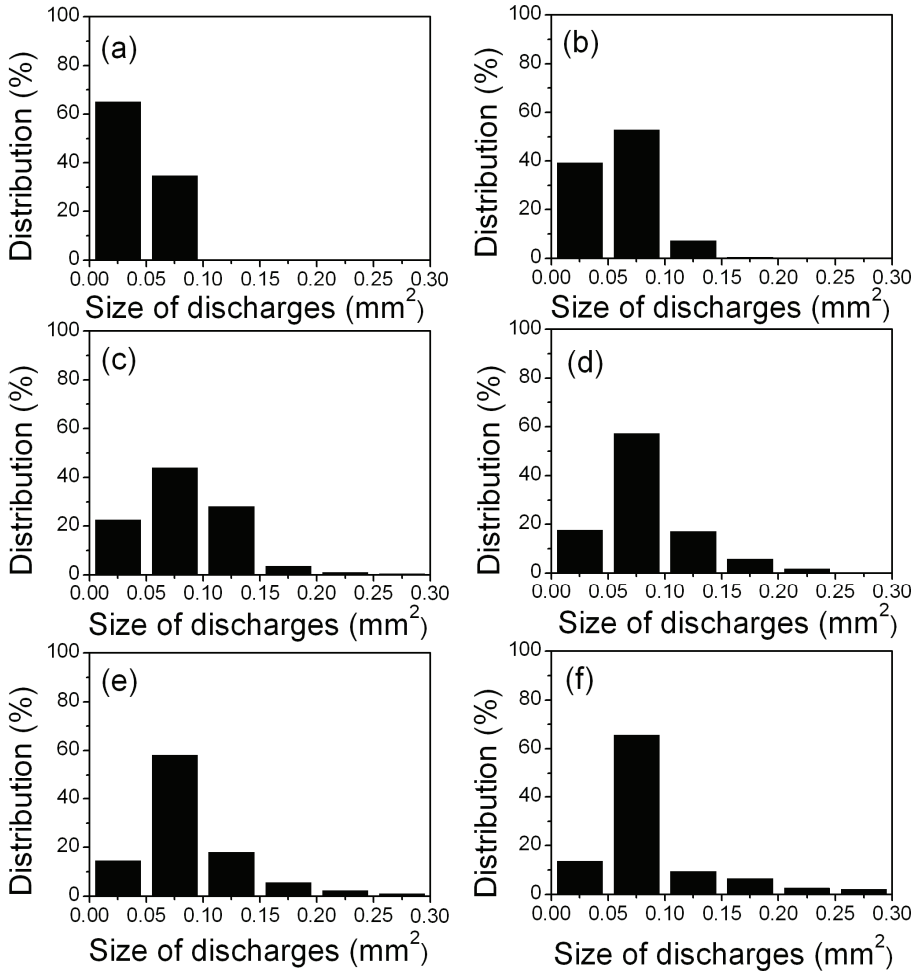


**Fig. 5** –The dimensional distribution of microdischarges at various stages of PEO process: (a) 2.5 min; (b) 5 min; (c) 10 min; (d) 15 min; (e) 30 min; (f) 45 min.

The increased size and decreased spatial density of microdischarges during PEO is related to the number of discharging sites through which higher anodic current is able to pass. The surface morphology evolution of the oxide coatings (Fig. 2), shows that the number of micropores decreases, while their size increases during PEO process. Also, thicker coatings have higher surface roughness (Fig. 6). In the initial stage of PEO, the discharge channels are well distributed and oxide coatings exhibit lower surface roughness. As the number

of discharge channels decreases with time of PEO, non-uniformities in the oxide coatings appear causing an increase in surface roughness. In a thicker layer of oxide coating, higher energy is required for the current to pass through. Under this condition, the current is localized at weak points of the layer formed to find its way through the oxide coating. This is the reason why the diameter of the discharge channel increases.

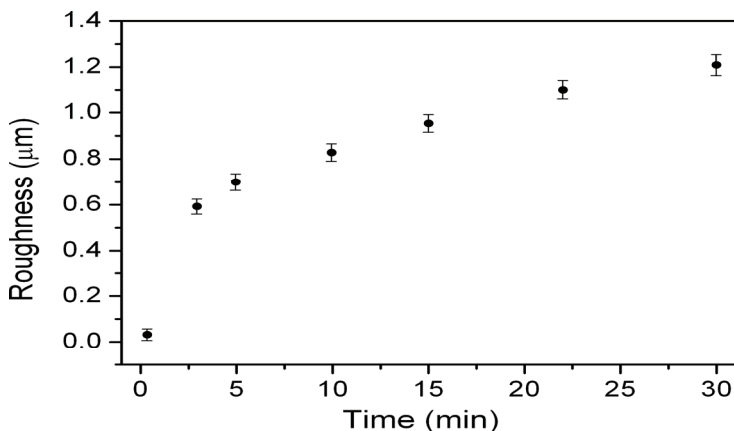


**Fig. 6** – Influence of PEO treatment time on roughness of oxide coating.

Typical optical emission spectrum of PEO microdischarges in the spectral region 380 nm to 850 nm is shown in Fig. 7a, while emission spectra in the range 380 nm to 480 nm and 700 nm to 850 nm are presented in Figs. 7b and 7c, respectively. Atomic and ionic lines were identified using the NIST online spectral database [12] and they belong to hydrogen and oxygen only. The strongest line is the  $H_{\alpha}$  (656.28 nm) while other two Balmer lines, the  $H_{\beta}$  (486.13 nm) and the  $H_{\gamma}$  (434.05 nm) are identified also. Strong lines are also O I at 844.62 nm, 844.64 nm and 844.68 nm. In addition, three O I lines at 777.19 nm, 777.42 nm, 777.54 nm and many other weaker lines of O I and O II are also detected (Fig. 7.) The notation I and II refers to neutral and singly ionized atoms, respectively. The continuum emission between 380 nm and 850 nm results from collision-radiative recombination of electrons and bremsstrahlung radiation [13]. The species that are identified originate only from the electrolyte, unlike in the case of PEO on aluminium [14]. Most likely, the absence of species originating from the substrate is caused by higher melting temperature of tantalum ( $\sim 3000$  °C), compared to melting temperature of aluminium (660 °C).

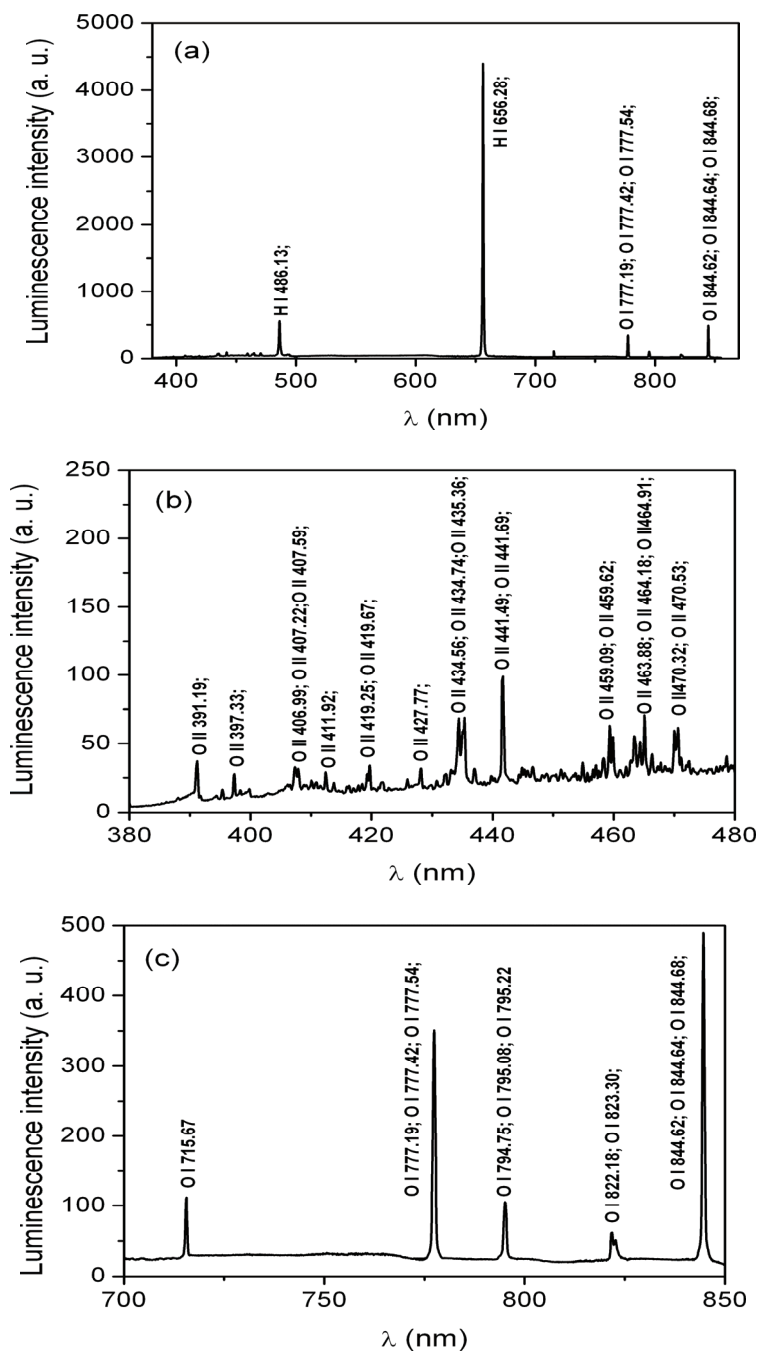


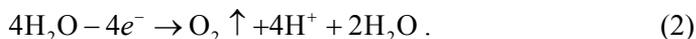
**Fig. 7** – Optical emission spectrum of PEO microdischarges in the spectral region: (a) 380-850 nm; (b) 380-480 nm; (c) 700-850 nm.

### 3.2 Chemical and phase composition of PEO coatings

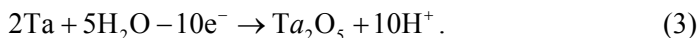
PEO is a complex process combining concurrent partial processes of oxide formation, dissolution and dielectric breakdown. At the beginning of tantalum anodization, oxide layer grows at the tantalum/oxide and oxide/electrolyte interfaces as a result of migration of  $O^{2-}/OH^-$  and  $Ta^{5+}$  ions across the oxide, assisted by a strong electric field. Also, small amounts of electrolyte are incorporated into the oxide at the oxide/electrolyte interface. The main chemical reaction at the tantalum/oxide interface is:



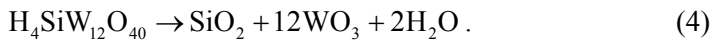
while the reaction at the oxide/electrolyte interface is:



The overall reaction is:



Under locally high temperatures and pressures that result from the influences of short-living microdischarges at sites of dielectric breakdown the following thermal decomposition of 12-tungstosilicic acid can be proposed:



SEM micrograph and EDS of two different regions on oxide coatings processed for 15 min are presented in Fig. 8. First EDS spectrum is taken in the region where the discharge takes place (Spectrum 1), while the other one is taken in the area around the discharge channel (Spectrum 2). Results of EDS analysis of surface coatings in Fig. 8 are shown in **Table 1**. Main elements of the coatings are Ta, O, Si and W. It is clear that the content of Ta is much higher in the discharge channels than in the surrounding area.

**Table 1**  
EDS analysis of oxide coating in Fig. 2.

	Weight (%)			
	O	Si	Ta	W
Spectrum 1	2.47	0.60	75.35	21.58
Spectrum 2	30.16		30.91	38.92

Influence of PEO treatment time on the chemical composition of oxide coatings is shown in Fig. 9. Clearly, the content of W increases during PEO, while the content of Ta decreases.

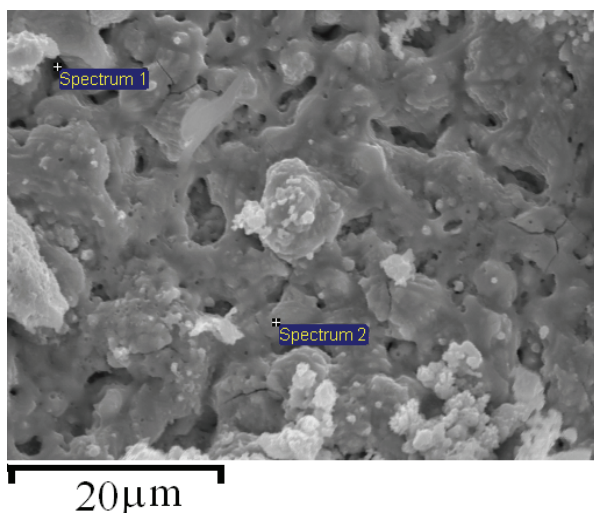


**Fig. 8** – SEM micrograph of oxide coating obtained by PEO process for 15 min.

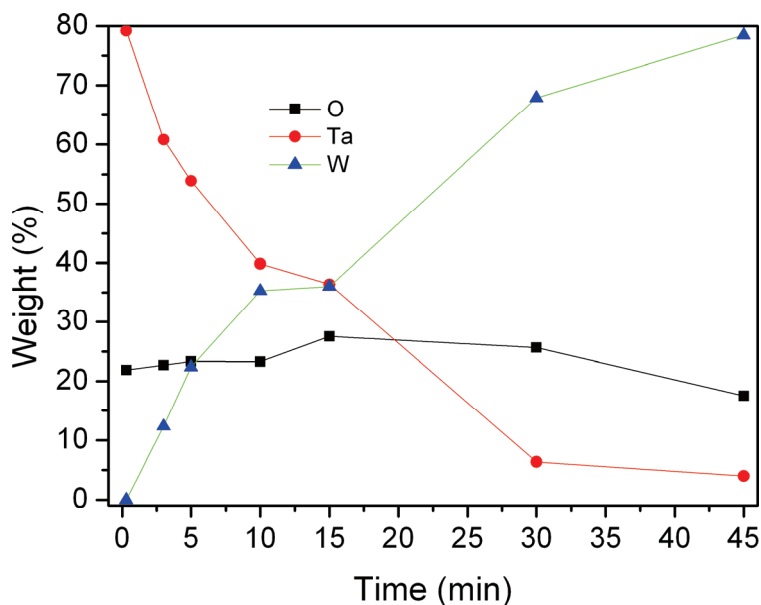


**Fig. 9** – Influence of PEO treatment time on the chemical composition of oxide coatings.

The XRD patterns of oxide coatings obtained after various anodization times are shown in Fig. 10. Before the breakdown, amorphous oxide film is formed (Fig. 10a). Elemental Ta mainly originates from the substrate and therefore Ta diffraction lines are strong. After the breakdown oxide coatings are

partly crystallized and mainly composed of  $\text{WO}_3$ ,  $\text{Ta}_2\text{O}_5$  and  $\text{SiO}_2$ . The content of  $\text{WO}_3$  increases with increasing time of PEO process, while content of  $\text{Ta}_2\text{O}_5$  and  $\text{SiO}_2$  decreases. Decrease of  $\text{SiO}_2$  in oxide coatings stems from the fact that stoichiometric ratio of Si to W atoms in 12-tungstosilicic acid (1:12) allows only small amount of Si to be incorporated in oxide coatings as  $\text{SiO}_2$ . Afterwards, the deficiency of available Si ions in the solution results in much lower amount of Si in oxide coatings (this process is diffusion limited). Both XRD and EDS data confirm this.

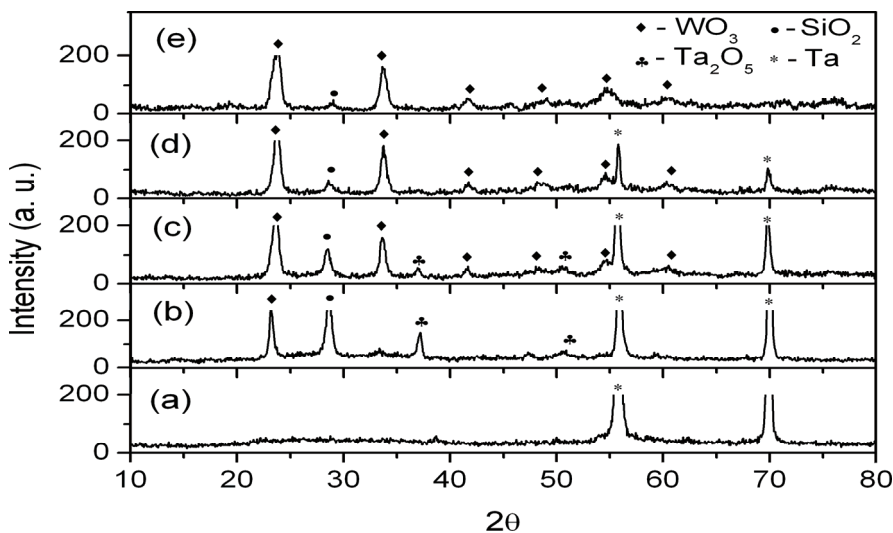


Fig. 10– XRD patterns of oxide coatings at various stages of PEO process: (a) 15 s; (b) 5 min; (c) 15 min; (d) 30 min; (e) 45 min.

#### 4 Conclusion

Plasma electrolytic oxidation (PEO) of tantalum was carried out in 12-tungstosilicic acid. The following conclusions were drawn:

1. The time and space distribution of microdischarges during PEO of tantalum is studied using real time imaging. The size of microdischarges becomes larger, while the number of microdischarges is reduced, with increasing time of PEO. Spatial density of microdischarges is the highest in the early stage of the PEO process. The percentage of oxide coatings area simultaneously covered by active discharge sites decreases slowly with extended PEO time.
2. Qualitative analysis of PEO emission spectra reveals that only H I, O I, O II and W I spectral lines are present.

3. The morphology, chemical, and phase composition of oxide coatings is investigated. The oxide coatings morphology is strongly dependent on PEO time. During the PEO of tantalum density of discharge channels decreases while their diameter increases, resulting in increased roughness of the oxide coating. The elemental components of PEO coatings are Ta, O, Si and W. The oxide coatings are partly crystallized and mainly composed of  $\text{WO}_3$ ,  $\text{Ta}_2\text{O}_5$  and  $\text{SiO}_2$ .

## 5 Acknowledgement

This work is supported by the Ministry of Education and Science of the Republic of Serbia under Project No. 171035.

## 6 References

- [1] F. Monfort, A. Berkani, E. Matykina, P. Skeldon, G.E. Thompson, H. Habazaki, K. Shimizu: Development of Anodic Coatings on Aluminium under Sparking Conditions in Silicate Electrolyte, *Corrosion Science*, Vol. 49, No. 2, Feb. 2007, pp. 672 – 693.
- [2] E. Matykina, R. Arrabal, P. Skeldon, G.E. Thompson: Transmission Electron Microscopy of Coatings Formed by Plasma Electrolytic Oxidation of Titanium, *Acta Biomaterialia*, Vol. 5, No. 4, May 2009, pp. 1356 – 1366.
- [3] R. Arrabal, E. Matykina, T. Hashimoto, P. Skeldon, G.E. Thompson: Characterization of AC PEO Coatings on Magnesium Alloys, *Surface and Coating Technology*, Vol. 203, No. 16, May 2009, pp. 2207 – 2220.
- [4] A.A. Voevodin, A.L. Yerokhin, V.V. Lyubimov, M.S. Donley, J.S. Zabinski: Characterization of Wear Protective Al-Si-O Coatings Formed on Al-based Alloys by Micro-arc Discharge Treatment, *Surface and Coating Technology*, Vol. 86-87, No. 2, Dec. 1996, pp. 516 – 521.
- [5] A.L. Yerokhin, X. Nie, A. Leyland, A. Matthews, S.J. Dowey: Plasma Electrolysis for Surface Engineering, *Surface and Coating Technology*, Vol. 122, No. 2-3, Dec. 1999, pp. 73 – 93.
- [6] X. Nie, E.I. Meletis, J.C. Jiang, A. Leyland, A.L. Yerokhin, A. Matthews: Abrasive Wear/corrosion Properties and TEM Analysis of  $\text{Al}_2\text{O}_3$  Coatings Fabricated using Plasma Electrolysis, *Surface and Coating Technology*, Vol. 149, No. 2-3, Jan. 2002, pp. 245 – 251.
- [7] S.V. Gnedenkov, O.A. Khrisanfova, A.G. Zavidnaya, S.L. Sinebrukhov, A.N. Kovryanov, T.M. Scorobogatova, P.S. Gordienko: Production of Hard and Heat-resistant Coatings on Aluminium using a Plasma Micro-discharge, *Surface and Coating Technology*, Vol. 123, No. 1, Jan. 2000, pp. 24 – 28.
- [8] J.W. Diggle, T.C. Downie, C.W. Goulding: Anodic Oxide Films on Aluminum, *Chemical Review*, Vol. 69, No. 3, June 1969, pp. 365 – 405.
- [9] K. Shimizu, G.E. Thompson, G.C. Wood: The Electrical Breakdown During Anodizing of High Purity Aluminium in Borate Solutions, *Thin Solid Films*, Vol. 92, No. 3, June 1982, pp. 231 – 241.
- [10] G. Sundararajan, L. Rama Krishna: Mechanisms Underlying the Formation of Thick Alumina Coatings through the MAO Coating Technology, *Surface and Coating Technology*, Vol. 167, No. 2-3, April 2003, pp. 269 – 277.

- [11] B. Kasalica, I. Belca, S. Stojadinovic, Lj. Zekovic, D. Nikolic: Light-emitting-diode-based Light Source for Calibration of an Intensified Charge-coupled Device Detection System Intended for Galvanoluminescence Measurements, *Applied Spectroscopy*, Vol. 60, No. 9, Sept. 2006, pp. 1090 – 1094.
- [12] [http://physics.nist.gov/PhysRefData/ASD/lines\\_form.html](http://physics.nist.gov/PhysRefData/ASD/lines_form.html).
- [13] S. Stojadinovic, R. Vasilic, M. Petkovic, Z. Nedic, B. Kasalica, I. Belca, Lj. Zekovic: Luminescence Properties of Oxide Films formed by Anodization of Aluminum in 12-tungstophosphoric Acid, *Electrochimica Acta*, Vol. 55, No. 12, April 2010, pp. 3857 – 3863.
- [14] J. Jovović, S. Stojadinović, N.M. Šišović, N. Konjević: Spectroscopic Characterization of Plasma during Electrolytic Oxidation (PEO) of Aluminium, *Surface and Coatings Technology*, Vol. 206, No. 1, Oct. 2011, pp. 24 – 28.